Dimensional Crossover in Ag Films Evaporated onto Angled Nanopore Array Substrates

Author: Ellen Royal

Advisor: Professor James Valles Jr.

A thesis presented for the degree of

Bachelor of Science

BROWN

Physics

Brown University

April 30, 2020

Abstract

Dimensional crossover has been achieved in a broad range of system types. Typically, the thickness of a film or the strength of a magnetic field is varied to force a transition from two dimensions to three or vice versa. Here, we propose a mechanism for observing one to two dimensional crossover by evaporating silver films onto angled anodic aluminum oxide substrates. This method of film fabrication creates an anisotropic array of metallic grains separated by insulating barriers. We predicted that because of the manner in which the angling of the substrate breaks the symmetry between the two axes of the film, the conductivity will be one dimensional along one axis and two dimensional along the other. We find that the resistance of a film evaporated onto an AAO substrate angled at 60° is two orders of magnitude different depending on the axis of measurement, suggesting that a dimensional crossover may have taken place. Further investigation will involve cooling the sample in order to use the temperature dependence of the conductivity to identify with certainty the system's dimensionality.

Acknowledgments

More people than I can count have helped me over the course of this project and in the years leading up to it. I would like to give special thanks to:

My father, for showing me "another failed experiment" was nothing to be ashamed of.

My mother, for always reminding me that not knowing how to do something and not being able to do it are not the same thing.

Gerald Zani, for being the first person at Brown to believe in me.

And, most of all, Professor Jim Valles, for his constant support, and for helping me learn to believe in myself.

Contents

List of Figures

1 Introduction

1.1 Quantum Corrections to Conductivity

Perhaps the simplest model of electrons in materials is the Drude model, which treats electrons as charged spheres, colliding with the other electrons and lattice sites in their path. The time between collisions is denoted as τ and the mean free path between collisions as λ. λ and τ are related by the Fermi velocity v_F such that $\lambda = v_F\tau$. In large, three dimensional conductors, the Drude model is sufficient to describe the collective behavior of electrons. In two dimensional and one dimensional systems, however, wave and quantum effects noticeably affect the electronic properties of the system. The most significant of these effects are localization, antilocalization, and interelectron interference, which influence the resistance of the material, and manifest differently in one and two dimensions. Based on prior research on these phenomena, we expect the temperature dependence of the resistance of 1D and 2D materials to be different, allowing us to use this measurement to determine the dimensionality of a novel system.

1.1.1 Localization

Classically, the probability that an electron will be found at a given point in space after a time $t >> \tau$ is given by

$$p(\mathbf{r}, t) = (4\pi Dt)^{-\frac{d}{2}} e^{-\frac{r^2}{4Dt}}, \quad \int p(\mathbf{r}, t) d\mathbf{r} = 1 \tag{1}$$

were d is the dimensionality of the system and $D = \frac{\lambda v_F}{d}$ is the diffusion coefficient [2]. However, localization and antilocalization make corrections to this classical probability which can be understood by analyzing the Feynman paths available to the electron. These paths are named for Richard Feynman, who was the first to use the uncertainty principle of quantum mechanics to describe the allowed trajectories of particles mathematically. In Feynman's model, when the state of a particle evolves in time, one sums each of its possible histories to obtain its present state.

In a pure, 2D crystalline lattice, all electron paths would be straight because the electron does not interact with a perfectly periodic potential. However, electrons will scatter off of

impurities in the material, which breaks this periodicity and introduces more complex paths. Therefore, included in the possible histories for the electron are closed loop paths, which return the particle to its original location. The particle can travel along the same closed loop in two different directions (Figure 1), and due to the wave nature of the electron, these so called "time reversed paths" interfere with each other.

If the phase shift of the electron wave function around the closed loop path is an integer multiple of 2π, the waves will interfere constructively, resulting in a higher probability of finding the electron at its initial location. This increased probability is known as weak localization because the electron wave function has become localized about this initial position rather than being spread out in space.

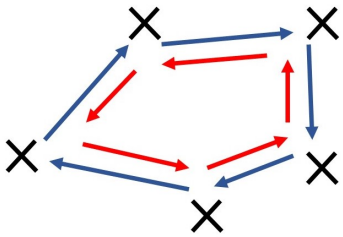

Figure 1: An electron scatters off of impurities (labeled with X's) and travels in a closed loop path in two opposite directions shown in red and blue.

If the wave functions interfere constructively, and we assume that their amplitudes $A_1 + A_2 = A$, the probability of finding the electron at its initial position is given by Equation 2.

$$|A_1 + A_2|^2 = |A_1|^2 + |A_2|^2 + 2|A_1 A_2| = 4A^2 \tag{2}$$

The probability given by quantum mechanics is twice the value given by classical mechanics, which is simply the sum of the squares of the two amplitudes. The resulting quantum probability function is shown in Figure 2.

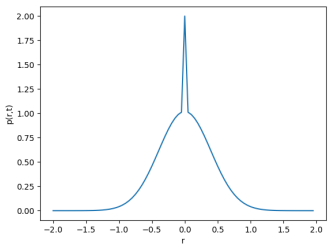

Figure 2: Probability function of the electron[2]. The center spike at r=0 is the result of constructive interference.

The probability function is given by the classical probability when $r \neq 0$, and the spike at r=0 represents the doubled probability to find the electron at the origin due to quantum interference effects. The spike has finite width due to the inherent uncertainty in the position of the electron, $\delta r \simeq \lambda$, where λ is the de Broglie wavelength of the electron. The area under the spike represents the total probability to find the electron at the origin. This area varies with time; as t

increases, the probability of finding the electron at the origin decreases.

Let us consider a small interval dt in which the electron can travel around all possible closed loop paths [2]. The elastic scattering time τ represents the shortest time interval in which the electron can travel around a closed loop path. However, electrons which take longer than this minimum time can still interfere with each other as long as they arrive back at the origin before the termination of the phase breaking time interval τ_φ. The phase breaking time interval accounts for the possibility that the electron, while travelling around the loop, will encounter a phonon or another electron which will alter its phase and prevent it from interfering with its time-reversed partner at the origin. The phase breaking time along with the speed of the electron sets the maximum volume of closed loop paths which the electron can travel and still return in time to undergo interference, $V_{loop} \propto \lambda^2 v_F dt$. The total distance travelled by the electron is given by $v_F dt$, and the factor of λ^2 is again the square of the uncertainty in the electron's position. At a given time, all the possible trajectories of the electron are confined within a volume whose magnitude is set by the diffusion constant D, the dimension of the space and the time t: $V_{any} \propto (Dt)^{\frac{d}{2}}$. In a thin film, which is an effectively 2D system, we let $d = 2$ but multiply by the thickness b of the film (which is assumed to be much less than the diffusion length $L_\varphi = \sqrt{D\tau_\varphi}$) to maintain the correct units. The probability any given electron's path is a closed loop is given by the ratio of these to volumes, $\frac{V_{loop}}{V_{any}}$. Integrating this ratio over the time interval τ to τ_φ yields the relative decrease in the conductivity of a 2D system due to localization (Equation 3).

$$\delta\sigma_2 \simeq -\sigma \int_\tau^{\tau_\varphi} \frac{v_F \lambda^2 dt}{(Dt)b} \simeq \frac{v_F \lambda^2}{Db} \ln \frac{\tau_\varphi}{\tau} \sigma \tag{3}$$

In a 1D system, localization effects are still due to interference between electron wave functions, however the mechanism is slightly different since clearly looped paths cannot exist in only one dimension. Instead, electrons encounter potential barriers at each impurity site and have some probability to either reflect off of the barrier or tunnel through (Figure 3).

As in the case of localization in two dimensions, there are many possible paths the electron can take involving transmission through and reflection off different combinations of potential barriers which will return it to its original position. Each interaction between the electron and a potential barrier introduces some small phase shift, and if the electron interacts with

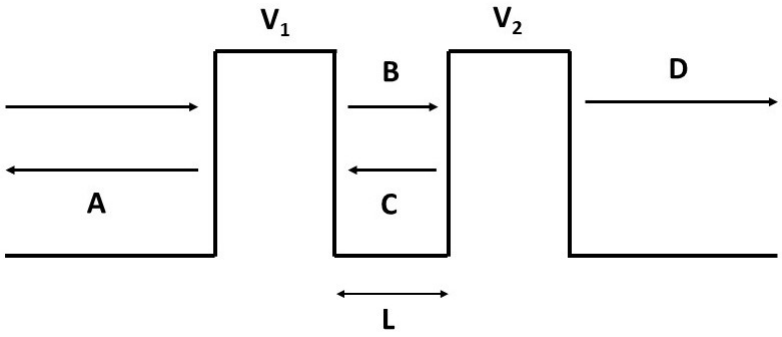

Figure 3: A wave incident on a series of potential barriers which has amplitudes A,B,C and D to be reflected or transmitted through the barriers

a long chain of impurities, these phase shifts are additive. If the total phase shifts along two or more paths which return the electron to the origin differ by integer multiples of 2π, the paths will interfere constructively, leading again to localization.

The decrease in conductivity due to localization can be quantified through an identical process to the 2D case, except we allow $d = 1$ and b is the diameter of the effectively one dimensional "wire" in which the electrons live (Equation 4). The volume of points from which the electron can reach the origin within the phase coherence time τ_φ is identical to the 2D case. However, from Equation 1, we see that the volume of points at which it is possible to find the electron at some arbitrary time t is given by $(Dt)^{1/2}$ in one dimension. We set up an almost identical integral to Equation 3 to find $\delta\sigma$ in 1D (Equation 4).

$$\delta\sigma_1 \simeq -\sigma \int_\tau^{\tau_\varphi} \frac{v_F \lambda^2 dt}{(Dt)^{1/2} b} = \frac{2 v_F \lambda^2}{D b^2} (\frac{L_\varphi}{l} - 1)\sigma \tag{4}$$

In the Drude model, the classical conductivity σ is given by Equation 5.

$$\sigma = \frac{n e^2 l}{\hbar k_F} \tag{5}$$

Subsituting Equation 5 into Equations 4 and 3 yields the absolute values of the corrections to the conductivity due to localization in 2D and 1D systems (Equation 6).

$$
\begin{aligned}
d = 2: \quad & \Delta\sigma_2 \approx -2(\frac{e^2}{\hbar})\ln(\frac{L_\varphi}{l}) \\
d = 1: \quad & \Delta\sigma_1 \approx -(\frac{e^2}{\hbar})\frac{L_\varphi}{l}
\end{aligned}
\tag{6}
$$

Though there is no explicit temperature dependence in Equation 6, both $\Delta\sigma_1$and$\Delta\sigma_2$ depend on the phase coherence length, L_φ, which in turn depends on the temperature. Interactions with phonons and other electrons are the chief causes of loss of phase coherence. However, as the temperature of a material decreases, both lattice vibrations and electron kinetic energies decrease, resulting in fewer collisions. Fewer collisions means the average time (or distance) an electron can travel without a phase-breaking interaction is much longer. Consequently, as $T \to 0$, the phase coherence length $L_\varphi \to \infty$. Effectively, $\Delta\sigma_1 \propto T$ while $\Delta\sigma_2 \propto \ln T$.

1.1.2 Antilocalization

In our discussion of localization, we neglected one fundamental property of electrons: spin. An electron has two possible spin projections: $+\frac{1}{2}$and$-\frac{1}{2}$. Because no spin measurement has taken place, the system behaves as if rather than a single electron, there are actually two, one with spin $+\frac{1}{2}$ and one with spin $-\frac{1}{2}$. Now consider both of these electrons traveling along a closed loop trajectory. As discussed in 2D localization, the electrons will traverse simultaneously every possible path around the loop, including pairs of identical paths traversed in opposite directions. As a result, it is now as if four electrons are traveling around the closed loop, two in one direction and two in the other, two with spin $+\frac{1}{2}$ and two with spin $-\frac{1}{2}$. The two spin-matched pairs are completely independent of each other, and the contribution to conductivity would follow the process outlined for localization, except that along the loop there is the possibility for one of these spins to flip. If a spin flips, the waves are no longer independent, and more complicated interference effects occur [2].

Electron spins can be caused to flip due to spin-orbit interaction. The magnetic moment μ of an electron moving with velocity v creates an electric field in the electron's rest frame. This electric field interacts with the electric field of the ions in the lattice, which leads to scattering. The strength of the spin-orbit scattering is proportional to $E_{ion}[\mu v]$, where E_{ion} is

the electric field of the ions in the lattice. E_{ion} is dependent on the size of the lattice nuclei, Z, and the fine structure constant, α, and therefore so is the spin-flip time τ_{so} (Equation 7).

$$\tau_{so} \propto (Z\alpha)^{-4} \tag{7}$$

However, because the spin flip time is much longer than elastic scattering time, $\tau_{so} >> \tau$, not every scattering event causes an electron spin to flip. Because of the dependence on atomic nuclei size, spin flips are more common in heavier metals, and therefore so are antilocalization effects.

Consider, again, two electrons traveling around a closed loop path in the same direction. There are two possible spin states for each of the electrons and consequently four possible states for the total spin of the electron pair: one with total spin-0, and three with total spin-1. The total interference is therefore a sum of the interference due to all four states. The wavefunction which describes the electron pair is given by Equation 8, where the superscripts (1) and (2) label the two different electrons and the subscripts (+) and (-) label the possible spin projections.

$$\Psi = \begin{bmatrix} \Psi_0 \\ \Psi_{1,-1} \\ \Psi_{1,0} \\ \Psi_{1,1} \end{bmatrix} = \begin{bmatrix} \frac{1}{\sqrt{2}}(\varphi_+^{(1)}\varphi_-^{(2)} - \varphi_-^{(1)}\varphi_+^{(2)}) \\ \varphi_-^{(1)}\varphi_-^{(2)} \\ \frac{1}{\sqrt{2}}(\varphi_+^{(1)}\varphi_-^{(2)} + \varphi_-^{(1)}\varphi_+^{(2)}) \\ \varphi_+^{(1)}\varphi_+^{(2)} \end{bmatrix} \tag{8}$$

The spin-orbit effect acts to rotate the electron spins [1] according to Equation 9.

$$V_{kk'}[1 + i\epsilon k \times k' \cdot s] = V_{kk'}[1 + iK \cdot s] \tag{9}$$

k and k' are the original and final electron wave vectors respectively, K is a three component vector which describes the rotation about the x, y and z axes. The total rotation of the spin s can be described by an operator R, such that $s' = R \cdot s$. The electron traveling in the opposite direction around the closed loop experiences the opposite spin rotation, and has a final spin described by s" $= R^{-1} \cdot s$. The inner product of these two spin vectors characterizes the interference effect. Ultimately, when a spin is flipped, a pair of electrons initially in the

triplet state will transition to the singlet state and vice versa. When $t > \tau_{so}$, many spin flips have taken place, so the electrons which were in the triplet state at $t = 0$ have transitioned to the singlet state.

Similarly to the case of localization, we arrive at the following expression for the correction to the conductivity (Equation 10):

$$\delta\sigma = \begin{cases} -\int_{\tau}^{\tau_\varphi} \frac{v\lambda^2 dt}{bDt}(\frac{3}{2}e^{\frac{-t}{\tau_{so}}} - \frac{1}{2})\sigma, & d = 2 \\ -\int_{\tau}^{\tau_\varphi} \frac{v\lambda^2 dt}{b^2\sqrt{Dt}}(\frac{3}{2}e^{\frac{-t}{\tau_{so}}} - \frac{1}{2})\sigma, & d = 1 \end{cases} \tag{10}$$

The $\frac{3}{2}e^{\frac{-t}{\tau_{so}}}$ term reflects the contribution to the conductance due to interference from the triplet components. The $-\frac{1}{2}$ term reflects the contribution due to the singlet component.

The triplet interference term is attenuated by the exponential factor and therefore is only relevant when $t < \tau_{so}$. Equivalently, the interference from the triplet components of the wave function is only relevant as long as the electron remembers its original spin. The factor of 3 accounts for the fact that the triplet state makes up three quarters of the total wavefunction. When $t << \tau_{so}$, the exponential approximates to 1, so as long as $\tau_\varphi << \tau_{so}$, we reproduce Equation 3, our original expression for the correction to conductivity due to localization. We would expect this result, because in this time interval, no spin flip has taken place which would lead to antilocalization.

When $\tau_{so} < t < \tau_\varphi$, the triplet interference term will go to zero, leaving only the contribution from the spin singlet. The sign of this term is negative because this component of the wave function is antisymmetric, resulting in a positive contribution to the conductivity. However, the overall sign of the quantum correction to σ depends on the relative sizes of the phase coherence time,which controls the strength of localization effects, and the spin-flip time, which controls the strength of antilocalization effects. If $\tau_{so} << \tau_{varphi}$, then many spin flips can occur before the electron loses its phase coherence, and antilocalization effects will dominate, resulting in a positive shift in the conductivity given by Equation 11.

$$
\begin{aligned}
d = 2: \quad & \Delta\sigma_2 \approx (\frac{e^2}{\hbar}) \ln(\frac{L_\varphi}{l}) \\
d = 1: \quad & \Delta\sigma_1 \approx \frac{1}{2}(\frac{e^2}{\hbar})\frac{L_\varphi}{l}
\end{aligned}
\tag{11}
$$

For films made up of smaller atomic nuclei, the quantum correction to the conductivity due to an electron's interference with itself will be localization, and the conductivity will decrease as explained in the previous section. However, in films made up of larger atomic nuclei, the conductivity due to an electron's interference with itself will be antilocalization, and the conductivity will increase. Here, we will investigate silver films with heavy atomic nuclei, so the dominant effect will be antilocalization.

1.1.3 Interelectron Interference

Quantum corrections due to localization and antilocalization are both caused by interference between different possible closed loop Feynman paths of the same electron. However, interference effects can also be observed due to interactions between different electrons - so called, interelectron interference.

Interelectron interference depends not on inelastic collisions but the difference in interacting electron energies ϵ_i. These initial energies determine the rate at which the electron's phase evolves with time, and it is the relative phase between two electrons which will determine the nature of the interference (Equation 12).

$$
e^{i\varphi(t)} = e^{i(\epsilon_i/\hbar)t} \tag{12}
$$

If an electron's energy lies in the range $\epsilon_F - T \leq \epsilon \leq \epsilon_F + T$, its motion is characterized by the diffusion equation (Equation 1). Two electrons subject to diffusion will have an average energy difference proportional to T, the temperature of the material. The coherence time, or the average time between interelectron interactions, τ_{ee} is given by Equation 13.

$$
\tau_{ee} \simeq \frac{\hbar}{T} \tag{13}
$$

The characteristic length scale, L_{ee}, is the size of the area in which interelectron interactions occur, and is determined by the coherence time (Equation 14).

$$L_{ee} \simeq l\sqrt{\frac{\tau_{ee}}{\tau}} \simeq \sqrt{\frac{\hbar D}{T}} \tag{14}$$

If electrons move with constant velocity along straight line paths with few scattering events, the average momentum transferred during a collision between two electrons is of the order of the Fermi momentum, k_F, the area in which the interaction takes place of the order $(k_F)^{-1}$, and the total interaction time of the order $\frac{\hbar}{e}$.

The temperature of the material determines the frequency with which electron collisions occur. Energy conservation demands that if the initial states of two interacting electrons lie within the energy range $\epsilon_F - T \leq \epsilon \leq \epsilon_F + T$, the final states must as well. As a result, the number of states available for an electron to scatter into is proportional to T. From the Drude model of electrons, the number of collisions between electrons is also proportional to T, so the probability for two electrons to collide is proportional to T^2. The rate at which collisions occur, $\frac{\hbar}{\tau_{ee}}$, is then proportional to $\frac{T^2}{\epsilon_F}$ with the factor of $\frac{1}{\epsilon_F}$ serving only to maintain proper dimensions.

However, the motion of electrons in materials is better described by a diffusion equation as in the discussion of weak localization. Diffusion brings electrons in proximity to each other more often than ballistic trajectories, meaning the area in which electrons interact, L_{ee}, is much larger than the $\frac{1}{k_F}$ hypothesized for mostly undisturbed trajectories. A large region for interaction means a smaller transfer of momentum, q. We can write τ_{ee} in terms of this momentum q, multiplying by the density of states to preserve dimensionality. The density of states is given by Equation 15.

$$g_d \propto \epsilon_F^{\frac{d}{2}-1}\sqrt{\frac{\hbar k_F}{v_F}} \tag{15}$$

q is proportional to the inverse of L_{ee}, so the rate of collisions between electrons in the diffusion model is proportional to $(g_d L_{ee}^d)^{-1}$. Because the density of states depends on d, the rate of collisions is different depending on the dimensionality of the system, and so too is the temperature dependence. Substituting in Equation 14 for L_{ee} and Equation 15 for g_d, the rate of collisions is given by Equation 16.

$$\frac{\hbar}{\tau_{ee}} = \begin{cases} T^{\frac{1}{2}}\tau^{\frac{-1}{2}}, & d = 1 \\ T\epsilon_F^{-1}\tau^{-1}, & d = 2 \end{cases} \tag{16}$$

From Equation 16, we see that the rate at which interelectron interactions occur decreases with a decrease in temperature. However, in 1D systems, the rate of interactions is proportional to the square root of the temperature, while in 2D systems the rate of interactions is proportional to temperature. This finding suggests that the corrections to conductivity produced by interelectron interactions will also have different temperature dependence based on the dimensionality of the system.

The probability that two electrons will take two paths which bring them to the same location in a time interval dt is the same as the probability that a single electron will take simultaneously two closed loop paths which arrive back at the same location in that time interval. Consequently, we can use the integral in Equation 3 from our discussion of localization with modified limits of integration. Instead of integrating up to τ_φ, consider the phase evolution as a function of time given in Equation 12. If the two interacting electrons have an energy difference of $\Delta\epsilon$ and are in phase at $t = 0$, then at $t = \frac{\hbar}{\Delta\epsilon}$, the difference in their phases will be of order one. Therefore, it is natural to choose $t = \frac{\hbar}{\Delta\epsilon}$ as the upper bound of our integration, because for higher values of t the electron pair will have lost all phase coherence (Equation 17).

$$\delta\sigma \approx -\sigma \int_{\tau}^{\frac{\hbar}{\Delta\epsilon}} \frac{v_F \lambda^2 dt}{(Dt)^{d/2} b} \tag{17}$$

The corrections to the conductivity are almost identical to those due to localization, but instead of depending on the interaction region L_φ, they depend on the interaction region L_{ee} (Equation 18).

$$\begin{aligned} d = 2: &\quad \Delta\sigma \approx -2(\frac{e^2}{\hbar}) \ln(\frac{L_{ee}}{l}) \\ d = 1: &\quad \Delta\sigma \approx -(\frac{e^2}{\hbar})\frac{L_{ee}}{l} \end{aligned} \tag{18}$$

L_{ee} is proportional to $\frac{1}{\sqrt{T}}$, so the correction to the conductivity in one and two dimensions depends differently on temperature. In 2D, $\Delta\sigma$ will increase proportional to $\ln T$, however

in 1D, $\Delta\sigma$ will decrease proportional to $T^{-1/2}$. The corrections due to antilocalization and interelectron interference will add to produce the total correction to the conductivity. In 2D, both corrections are proportional to $\ln T$, so the total conductivity will be as well. In 1D, however, the relationship is slightly more complicated, as we see the strength of antilocalization depends on T while the strength of interelectron interference depends on $T^{-1/2}$.

This temperature dependence has been verified experimentally. Shown in Figure 4 is a linearized plot of the change in conductance, ΔG (scaled for ease of viewing) for a variety of 2D copper films as a function of $\ln T$ [10]. Note that the plots shown are taken for the change in conductance in the weak localization, rather than antilocalization, regime, however the dependence of the magnitude of ΔG on T for the two processes is identical.

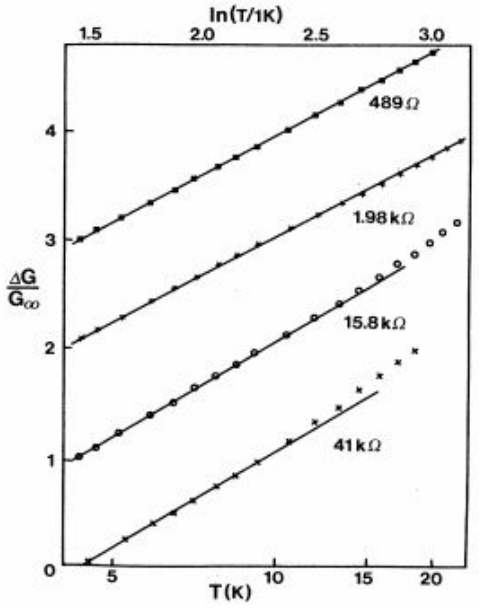

Figure 4: Plot of change in conductance, ΔG, as a function of $\ln T$ for various two dimensional Cu films [10]

The total change in conductance of a 1D film has a more complex temperature dependence and is therefore more difficult to fit. However, if the conductance as a function of T is approximately linear at high temperatures and the conductance as a function of $\ln T$ is not linear, we can safely assume that the film is one dimensional.

1.2 Evidence for Dimensional Transitions

Though it is impossible to create a truly one or two dimensional film, a film will behave as if it is of a lower dimension if the characteristic length scale describing interactions within the material is much greater than the film thickness. Therefore, dimensional crossover can be achieved by altering either the film thickness [6] or the characteristic length scale with, for example, a magnetic field [7].

However, more elaborate methods have been developed to achieve dimensional crossover

which rely on the quantum nature of electrons discussed in the above sections. In multilayer films, for example, dimensional crossover is observed as a result of quantum tunneling [4]. When two conducting layers of $Nb_{0.53}Ti_{0.47}$ are separated by an insulating layer of Ge, depending on the thickness of the Ge layer, the material will behave as if it were three dimensional or two dimensional depending on the thickness of the Ge layer. If the Ge layer is thinner than 30 Å, electrons in the conducting layers will have finite probability to tunnel through from one conducting layer to the other, and the material is effectively three dimensional. However, if the Ge layer is thicker than 30 Å, tunneling is suppressed and the conducting layers will each behave as if they are 2D.

Here, we propose a similar method of dimensional crossover. Electrons, rather than being confined to conducting layers, can be confined to conducting "islands" separated by an insulating "sea". The probability for an electron to hop from one atom to an empty orbital in a nearby atom decays exponentially with the distance between the atoms[5]. The relationship between hopping probability and atomic distance is given by Equation 19, where R is the distance between atoms, k_B is Boltzmann's constant, T is the temperature of the system, ΔE is the energy difference between the two orbitals, and ξ gives the decay of the wavefunction due to a potential barrier.

$$P \propto \exp\left(\frac{-2R}{\xi} - \frac{\Delta E}{k_B T}\right) \tag{19}$$

When the islands are close together, the electrons are free to tunnel through the potential barrier which separates them and the sample will conduct. However, because the hopping probability decays exponentially with an increase in atomic distance, there is very little probability for the electrons to hop between widely spaced islands. When the islands are spaced far apart, the electrons will no longer be able to tunnel, and the sample will be an insulator. If it is possible to fabricate an array of metallic islands which are widely spaced in one direction but closely spaced in another, electrons will prefer to move in the direction of the closely spaced wells. When electrons are induced to travel along the row of islands, very little hopping between rows will be observed, and the material will be effectively one dimensional. However, if an applied potential difference gives electrons enough energy to hop between rows, they are now free to move along both directions, and the material will

be effectively two dimensional. The conductivity of the material along the direction of the closely spaced islands will be different, consequently, than the conductivity along a direction perpendicular to the islands, allowing a dimensional transition to be observed.

1.3 Fabrication of Thin Films

While measuring the dimensionality of an existing film is relatively straightforward, it remains to be shown that it is possible to engineer a film which can be expected to behave as if it is two dimensional under some conditions and one dimensional under others.

Fabrication of thin films by evaporating metal onto a substrate is characterized by a nucleation process in which atoms deposited on the substrate surface coalesce into larger grains. This process progresses differently depending on the nature of the substrate. Here we consider first film formation on flat substrates and then on porous anodic aluminum oxide (AAO) substrates where we expect the dimensional cross over to occur.

1.3.1 Fabrication and Behavior of Films on Flat Substrates

On a flat substrate, when atoms arrive at the substrate surface, they diffuse away from the original point of impact according to Equation 20 [9].

$$\langle x^2 \rangle = Dt \tag{20}$$

The diffusion constant D is determined by the temperature of the substrate, T, the diffusion activation energy E, and a constant D_0 which is related to the vibrational frequency of the atom (Equation 21).

$$D = D_0 e^{\frac{-E}{k_B T}} \tag{21}$$

Alternatively, atoms deposited on the substrate surface have some probability of desorbing, or being released from the substrate. As long as the activation energy of desorption is less than the activation energy of diffusion, the atoms will diffuse and larger grains can form. The process of forming larger grains is related to the surface energies - the excess energy at the surface of the material relative to the bulk - of three different boundaries:

the film-substrate boundary, film-vapor boundary, and the vapor-substrate boundary [11]. These energies can also be thought of as surface tension vectors. The substrate-vapor surface tension pulls against the film-substrate and vapor-film surface tensions, and the three are in equilibrium when Equation 22 is satisfied.

$$\gamma_{sv} = \gamma_{fs} + \gamma_{vf} \cos\theta \tag{22}$$

Here, θ represents the contact angle between the grain and the substrate, and is determined entirely by the other three parameters. If γ_{sv} is larger than γ_{fs}, the system will seek to reduce its energy by spreading the grain out across as much of the substrate as possible to minimize the area of the substrate-vapor interface and maximize the film-substrate interface. If γ_{sv} is smaller than γ_{fs}, however, the grain will seek to leave as much of the substrate-vapor interface exposed as possible, forming a large, round grain, as in Figure 5. For wetting to occur, θ must go to zero, which is true as long as $\gamma_{sv} > \gamma_{fs} + \gamma_{vf}$.

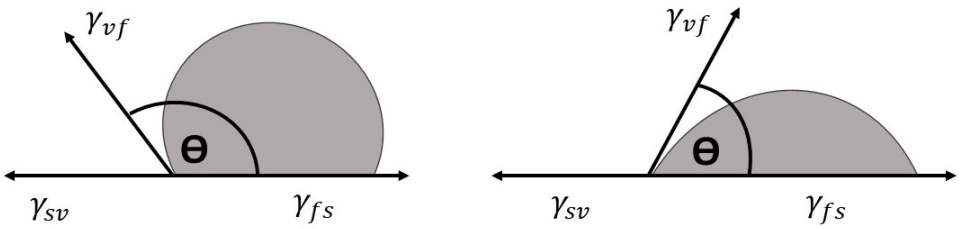

Figure 5: Contact angle between grain and surface.

However, if the surface energies are such that wetting does not occur, grains will form as atoms diffuse across the substrate surface and bind together. We assume here that once atoms bind to a grain, they cannot break free, which is not always true at high temperatures.

1.3.2 Fabrication and Behavior of Films on Anodic Aluminum Oxide Substrates

Thin films deposited on anodic aluminum oxide (AAO) substrates have unique properties due to the porous nature of the substrate. The oxide layer is insulating and characterized by a highly ordered array of pores a few micrometers deep and nanometers in diameter. Grains collect in the pores as shown in Figure 5.

Initially, as atoms are deposited, the grains adhere to the sides of the pore and do not fill the opening. As gaseous metal atoms continue to strike the substrate, the grains grow in size in much the same way as they would on a flat substrate, eventually merging with each other. By the time the film thickness reaches approximately 15 nm, the small grains have coalesced into one large grain which fills the mouth of the pore. When the film reaches approximately 25 nm, the central grain has grown larger than the mouth of the pore, and grains begin to form in the space between pores.

Whether grains collect in the mouths of the pores is determined by the surface energies of the three relevant interfaces: film-substrate, film-vapor, and vapor-substrate. Because the atoms coalesce into large, well defined grains, the surface energies must comply with the inequality determined by Equation 21. However, the fact that the grains collect in the pore mouths rather than between the pores implies this configuration must be the most energetically favorable. To see this, consider the free energy difference, Δg, between two grains of identical size, one in the mouth of a pore and one adhering directly to the substrate in between pores [8] (Equation 23).

$$\Delta g = [\gamma_{fs} a_{fs} + \gamma_{vf} a_{vf}] - [\gamma_{vf}(a_{fs} + a_{vf}) + \gamma_{sv} a_{fs}] \tag{23}$$

In Equation 23, a_{fs} refers to the area of the film-substrate interface and a_{vf} refers to the area of the vapor-film interface of a grain which forms in the region between pores. The first term then represents the energy of such a grain. The second term gives the energy of a grain with the same total surface area, $(a_{fs} + a_{vf})$, in the mouth of a pore.

The origin of the first term is fairly obvious. To arrive at the second term, we first assume that the area of the vapor-film interface is now approximately equal to the total surface area of the grain, so the energy of the grain surface is $\gamma_{vf}(a_{fs}+a_{vf})$. However, in moving the grain from the substrate to the mouth of the pore, we have exposed an area of the substrate surface equal to a_{fs}, so we add the surface energy of this new substrate-vapor interface, $\gamma_{sv} a_{fs}$, to the total energy. Combining the two expressions, we arrive at the second term in Equation 23. If grain coalescence in the mouth of a pore is to be energetically favorable, Δg must be greater than zero, requiring $\gamma_{sv} < \gamma_{fs} + \gamma_{vf}$, the same condition as for nonwetting. As a result, any metal which does not wet the surface of the substrate will tend to collect in the

pore mouths.

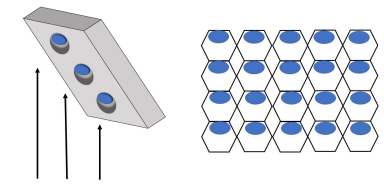

(a) (b)

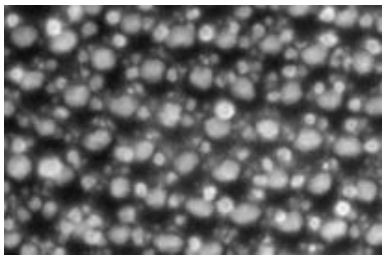

(c)

Figure 6: Mechanism of grain coalescence in angled substrate: (a) Flux of evaporated atoms collecting in pores of angled substrate; (b) Grains coalesced asymmetrically in pores; (c) SEM image of 15 nm Pb film evaporated onto AAO substrate held at 60°[11]

Films of approximately 15 nm are ideal to create the desired ordered array of metallic grains which we hope to manipulate in order to induce a dimensional crossover. At this film thickness, grains are either in contact with their neighbors or closely spaced enough to enable electrons to tunnel between them. Films of thickness less than 15 nm will struggle to conduct because of the large stretches of insulating substrate between the metallic grains, making them poor candidates for studying dimensional crossover since it is the relationship between conductivity and temperature of the film which will reveal its dimension. Films with thickness greater than 15 nm will conduct more easily, however the film possesses no universal order which could be manipulated to distinguish one dimension from another.

If the substrate is oriented at some angle to the incoming flux of evaporated atoms, the isotropy of the well array will be broken [11]. Angling the substrate will cause the grains to coalesce in the pores asymmetrically, creating a gap between the rows of metallic wells in one direction while holding the well spacing constant in the other (Figure 6). This gap reduces the overlap between electron wavefunctions between rows, which discourages electrons from hopping from one row to another, as dictated by Equation 9. Therefore, we expect that if the conductivity is measured along the axis of the closely spaced wells, the electrons will be confined to a single row, and the film will behave as if it were one dimensional. However, if the conductivity is measured along the perpendicular axis, the electrons may still travel left and right along the same row, but will have no choice but to hop between rows as well, causing the film to behave as if it is two dimensional.

2 Experimental Methods

2.1 AAO Fabrication

AAO substrates were fabricated in Professor Jimmy Xu's lab from aluminum strips in four stages: electropolishing, first anodization, oxide layer removal, and finally a second course of anodization. At all stages, the temperature of the solution had to be carefully maintained [3].

The electropolishing stage required the strip to be submerged for just 5 minutes in a perchloric acid and ethanol solution held at 0°C. During the electropolishing, the aluminum strip was held about 1.5 cm away from and facing a piece of graphite. The aluminum served as a cathode and the graphite as an anode as a 15V potential difference was applied across the two, causing ions in the solution to flow between the two materials and break down any oxide or oil that had accumulated on the surface of the aluminum strip.

After electropolishing, the strip and the graphite were cleaned with ethanol, reinforced with teflon tape, and transferred to a 0.3M oxalic acid solution held at 0°C for anodization for 16 hours. The strip still served as a cathode and the graphite as an anode with the same approximate spacing between them, however the potential difference was increased to 40V.

The first anodization left a porous oxide layer on the surface of the aluminum, however the pore arrangement was nonuniform, and the possibility for one dimensional conductivity required evenly spaced rows of pores. Consequently, the oxide layer had to be removed using a phosphoric acid and chromic oxide solution. The aluminum strip was suspended in the solution held at 60°C for 24 hours to ensure the oxide layer was fully dissolved. No graphite electrode or potential difference was required for this stage.

A second anodization was then completed to establish an oxide layer comprised of a more uniform array of pores on the surface of the aluminum. The same solution, temperature, and potential were used as in the first anodization. However, to create pores which were 6 μm deep, the strip was left to anodize for only 1 hour. After anodization, the strip was examined using an SEM microscope to ensure that the pore array was satisfactory.

2.2 Evaporation

Metal was evaporated onto the substrate using an Edwards 306 evaporator evacuated to 2×10^{-6} torr. The solid metal was held in a wire basket and a large current (24-28 A) was put through the wire, raising its temperature and causing the metal to evaporate. The AAO substrate was cleaned thoroughly with methanol and de-ionized water to ensure no dust had collected on the surface which would interfere with the film formation and attached to a sample holder with vacuum grease. The sample holder was positioned about 15 cm above the basket such that the atoms of the gaseous metal as they travel balistically upwards into the chamber would collect on the surface.

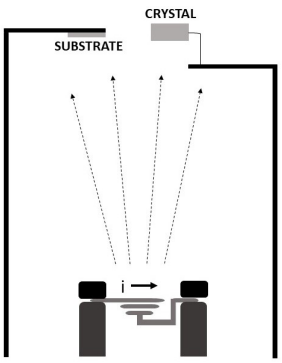

Figure 7: Schematic of evaporation of metal onto crystal and substrate.

The thickness of the film was monitored using a quartz crystal held adjacent to the sample holder so that roughly the same number of atoms/unit area would adhere to the crystal surface as the substrate (Figure 7). The crystal is wired in a circuit that causes it to oscillate with a stable resonant frequency of about 5 MHz. However, as metal accumulates on the surface of the crystal, its resonant frequency decreases. The rate of decrease is different depending on the metal, but if this relationship is known, it is possible to determine the thickness of the film deposited on the crystal and therefore, indirectly, the thickness of the film deposited on the substrate. Here, we apply a 10V potential difference to the circuit and measure the resonant frequency with a Tektronix DC510 frequency counter. The output of the counter was digitized by a Keysight USB2.0/GPIB Interface and plotted as a function of time on a computer using Labview software to monitor the film thickness during evaporation.

Film fabrication took place in three stages. First, a 10 nm germanium base layer was added to the entire substrate with the substrate held perpendicular to the flux of incoming germanium atoms. The germanium was used to smooth the oxide surface so more uniform films could be evaporated later.

During the second and third stages, masks were placed over the substrate to restrict the regions to which evaporated atoms could adhere. The mask used in the second stage

determined the location of the contacts which would be used to evaluate the conductivity of the film. The mask used in the third stage determined the size and orientation of the films.

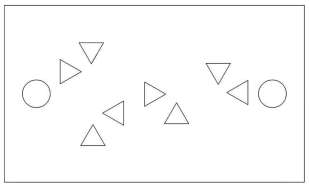

(a)

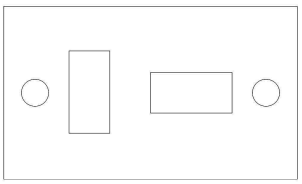

(b)

Figure 8: (a) mask placed over substrate to evaporate contacts (b) mask placed over substrate to evaporate films

Both masks were designed such that the tips of the contacts would overlap with the films and such that the two films and sets of contacts would be identical in size but rotated 90 degrees relative to each other (Figure 8). This orientation was chosen so that the voltage across one film would be measured in the direction parallel to the widely spaced rows of metallic wells and the voltage across the other would be measured in the direction perpendicular. As a result, one film, hypothetically, should behave as a two dimensional conductor and the other as a one dimensional conductor.

The contacts were made by evaporating 10 nm of silver with the substrate still oriented perpendicular to the flux of incoming silver atoms. Gold wires were attached to the evaporated contacts with silver paint, both of which were chosen for their low resistances. The sets of triangular contacts on each of the film ends were used to run current, while the two in between were used to measure voltage. (The circles on either end of both masks were used to affix the mask on top of the substrate and did not contribute to contacts or films.) The contact spacing was held constant for both films because the potential difference between two points on the film depends on the distance between them.

The silver films were made last, with the substrate oriented either perpendicular to the incoming flux of silver atoms (the control condition), or at a 60° angle. The films had to be 15 nm thick to create the desired array of metallic wells, but when the substrate was angled, $\frac{15}{\cos 60} = 30$nm worth of silver actually had to be evaporated to create a 15 nm film.

2.3 Resistance Measurement

The two films were wired in series with a 3007 Ω resistor (Figure 9) and the voltage across all three circuit elements was measured as a function of time during the film evaporation. The voltage across the known resistor was used to determine the current in the circuit via Ohm's law: $V = IR = I(3007\Omega)$. Wiring the three elements in series ensured that the current through the 3007 Ω resistor was the same as the current through both of the films. Plugging the calculated value of the current into Ohm's law with the measured voltage drop across each film, it was possible to determine each of the film resistances either as a function of film thickness or as a function of temperature.

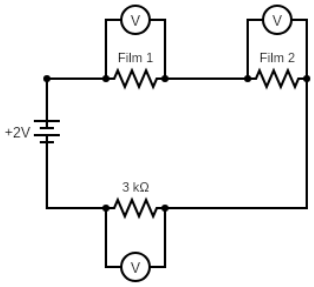

Figure 9: Circuit diagram of two films wired in series with 3007 Ω resistor

This indirect method of resistance measurement was necessary to improve accuracy. A direct, two terminal resistance measurement would return not only the resistance of the film, but also that of the ohmeter's probes and wires. Measuring the voltage drop across the film with a second pair of wires removes these errors. Because the voltmeters and the films are wired in parallel, the voltage drop across both will always be identical regardless of the voltmeter's resistance, giving the true value of the voltage as opposed to an offset value of resistance.

The actual measurements were taken using an National Instruments USB-6009 Data Acquisition Card Module. This device acted as a variable power supply to run current through the circuit as well as a voltmeter to take voltage measurements across the 3007 Ω resistor and the films. The NI USB-6009 communicated directly with the Labview computer software, allowing voltage measurements to be taken as a function of time while the film was evaporating, so the resistance of the film as a function of film thickness could be determined.

2.4 Temperature Variation

After creating the films, the evaporator was pumped down to about 5×10^{-5} torr and the films were slowly cooled by running liquid nitrogen through a metal tube. The tube was

embedded in a copper plate and attached to the plate was a thin braid of copper wire which could be affixed to the sample holder with a screw. Over time, the nitrogen cooled the copper plate, the braid, and the sample holder.

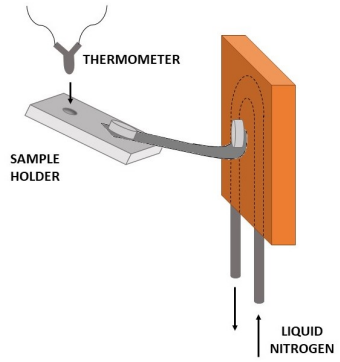

Figure 10: Diagram of mechanism for cooling films and measuring temperature

The temperature of the film was monitored with a platinum thermometer which sat in a small hole in the back of the sample holder. The resistance of the thermometer was measured as a function of time and its temperature was known. As the films were cooled, the voltage drops across the thermometer and the films were measured as a function of time (Figure 10).

The resistance of the thermometer was determined using a similar circuit to that in Figure 9. A 1 MΩ resistor was wired in series with the thermometer and the voltage drop across this resistor was used to determine the current in the circuit. From the current and the voltage drop across the thermometer, it was possible to calculate the thermometer's resistance as a function of time. The same NI USB 6009 Module and Labview program was used to collect and analyze data. The resistance of the thermometer was then used to determine its temperature, and the relationship between temperature and resistance of the two films could be plotted to determine the film's dimension.

3 Results and Analysis

Sample plots of crystal resonant frequency and film thickness as functions of time during evaporation of a 1 nm silver film are shown in Figure 11.

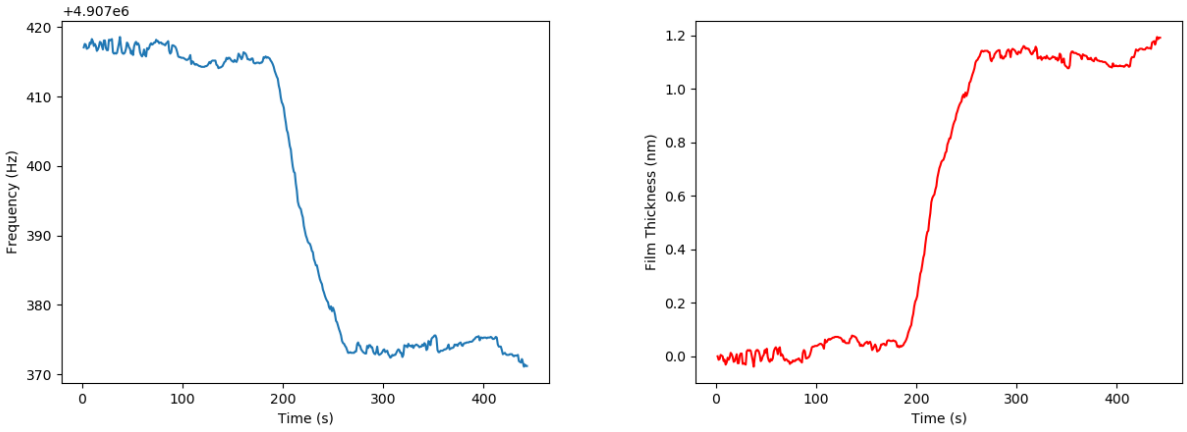

(a) (b)

Figure 11: During evaporation of approximately 1 nm silver film: (a) plot of crystal resonant frequency vs. time; (b) plot of film thickness versus time

The primarily flat regions of the two plots in Figure 11 occur when current flows through the wire basket but it has not reached the necessary temperature for metal to evaporate and after the current has been reduced and the basket has begun to cool, causing evaporation to cease. Small fluctuations in these regions are due to natural fluctuations in crystal frequency, not irregularities in evaporation. During the evaporation, the thickness of the metal deposited on the crystal surface increases almost linearly with time.

Before angling the substrate, a set of control films was evaporated on a flat substrate. The film thickness was 20 nm, and the NI USB 6009 was set to produce a 2V potential difference to drive the circuit. The voltage measurements for the three circuit elements under these conditions are given in Table 1.

Using the voltage drop across the known shunt resistor in Ohm's law yields a current value of 9.41×10^{-6} Amps through the circuit. This current value along with V_1 and V_2 were then used to calculate the resistances of the two films (Equation 24).

Circuit Element	Voltage (V)
Resistor	2.83×10^{-2}
Film_1	2.9×10^{-4}
Film_2	5.29×10^{-4}

Table 1: Voltage measurements across shunt resistor and films evaporated onto substrate held at 0°

$$\begin{aligned} \frac{I}{V_1} &= \frac{9.41 \times 10^{-6}}{2.9 \times 10^{-4}} = R_1 = 30.8\Omega \\ \frac{I}{V_2} &= \frac{9.41 \times 10^{-6}}{5.29 \times 10^{-4}} = R_2 = 56.2\Omega \end{aligned} \tag{24}$$

On the flat substrate, there is some disparity between the resistances of the two films, but it is likely due to the nonuniformity of the AAO substrate, not any difference in dimensional behavior of the two films. SEM images of the substrate could say more about the reasons for the slightly different resistances of the two films.

The sample of AAO used for evaporation onto the angled substrate is shown in Figure 12. The pore array, unfortunately, is not nearly as uniform as we had hoped. The rows are evenly spaced and parallel in discrete regions of the substrate, however the rows in different regions are angled relative to each other. This nonuniformity, while potentially contributing to differences in the resistances of the two films, will in all likelihood decrease the prominence of the dimensional transition. The cause of this nonuniformity is unclear. However, the aluminum strip was damaged during the second anodization process in which the ordered pore array is formed, which could have caused this nonuniformity. During the second anodization, if the temperature of the solution was not constant throughout, the anodization may have progressed more quickly at the surface of the solution, thereby eroding the strip. The erosion may have interfered with the completion of the anodization process, leaving the pores nonuniform.

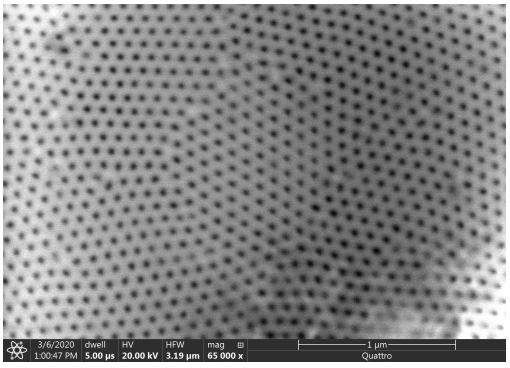

Figure 12: SEM image of AAO substrate after two stage anodization

The voltage drops across the two films evaporated onto this sample of AAO, held at an angle of 60°, were drastically different. The voltage drops across the shunt resistor and two 15 nm silver films are given in Table 2, with the NI USB 6009 producing a 2V potential difference to drive the circuit. Here, $\text{Film}_{\parallel}$ refers to the film where the voltage is measured parallel to the widely spaced rows and $\text{Film}_{\perp}$ refers to the film where the voltage is measured perpendicular to the rows, and the resistor refers to the 3007 Ω shunt resistor.

Circuit Element	**Voltage (V)**
Resistor	2.87×10^{-2}
$\text{Film}_{\parallel}$	4.61×10^{-1}
$\text{Film}_{\perp}$	4.39×10^{-3}

Table 2: Voltage measurements across shunt resistor and films evaporated onto substrate held at 60°

Plugging the voltage across the known resistor into Ohm's law yields a value of 9.56×10^{-6} Amps for the current. Plugging this current into Ohm's law along with $V_{\perp}$ and $V_{\parallel}$ (the voltage drops across films oriented perpendicular and parallel to the widely spaced rows respectively), the resistances of the two films are given in Equation 25.

$$\begin{aligned} \frac{I}{V_{\perp}} &= \frac{9.56 \times 10^{-6}}{4.39 \times 10^{-3}} = R_{\perp} = 4.60 \times 10^{2}\Omega \\ \frac{I}{V_{\parallel}} &= \frac{9.56 \times 10^{-6}}{4.61 \times 10^{-1}} = R_{\parallel} = 4.82 \times 10^{4}\Omega \end{aligned} \tag{25}$$

From Equation 25, we see that the resistances of the films differ by two orders of magnitude, while the resistances of the control films only differed by a few Ohms. Some of this discrepancy could be due to nonuniformity of the substrate, though likely this would not have produced such a dramatic effect. An additional contribution could have come from nonuniformity in the contacts. We found that evaporating films onto an angled substrate shifted the location of the films a millimeter or more upwards from the expected location because of the small separation between the mask and the substrate. As a result, gaps opened up between the films and some of the contacts, which were evaporated onto a horizontal substrate

and therefore did not experience the same shift. (To avoid this problem in the future, the contacts should be evaporated at the same angle as the films.) The contacts were modified afterwards by applying small drops of silver paint to fill these gaps, meaning that the final contact spacing for the two films could have been slightly different, which would have influenced their measured resistances. However, the contacts were shifted at most by a fraction of a millimeter, which would not likely account for a difference of two orders of magnitude in the resistances of the films, which suggests that it is the angling of the substrate during evaporation and the formation of widely spaced rows that caused this large discrepancy.

Intuitively, we could expect the resistance of the film along the direction of the rows of closely spaced grains to be smaller, as hopping between rows requires more energy than traveling along them. However, in this trial, we find instead that $R_\perp$ is much smaller than $R_\parallel$. It is not clear at this point why the ratio of the resistances of the two films differs from expectation. Some possible explanations could be the grains along the rows are not as closely spaced or the rows are closer together than we had predicted. SEM images of the grain configuration could provide more information. Cooling the films will also be necessary to reveal whether this difference is a result of dimensional crossover.

4 Conclusions

In this investigation, we considered the difference in temperature dependence of the quantum corrections to conductivity in one and two dimensions as a means of determining the dimensionality of a novel system. We studied 15 nm silver films evaporated onto anodic aluminum oxide substrates angled at 60° to the vertical. The substrate consists of a nearly isotropic configuration of pores, which lead to a uniform array of metallic grains when a metal is evaporated onto a completely horizontal substrate. When the substrate is angled, metal collects asymmetrically in the pores, leading to an array of grains which are closely spaced along one axis of the film and widely spaced along the other. We predicted that the conductivity along the axis of the closely spaced grains would be one dimensional, while the conductivity along the perpendicular axis would be two dimensional.

While we did not find concrete proof of a dimensional transition, we have evidence to suggest that films behave differently when the conductivity is measured along the axis parallel to the rows of grains versus the axis which is perpendicular. On flat substrates, the resistances measures along two perpendicular axes were within an order of magnitude of each other. On the angled substrate, these resistances differed by two orders of magnitude. This finding suggests that angling the substrate breaks some symmetry between the axes and causes them to conduct differently. However, we did not confirm that this change in conductivity is a result of a dimensional transition.

Subsequent investigations should focus on cooling films evaporated onto AAO substrates angled at 60° to generate plots of $R_\perp$ and $R_\parallel$ as a function of temperature. From the analysis of quantum corrections to conductivity, we know that the conductivity, which is proportional to the inverse of resistance, has a different T dependence depending on the dimension of the system. In two dimensions, antilocalization effects and interelectron interference result in a positive correction to the conductivity proportional to $\ln T$. Alternatively, in one dimension, antilocalization results in a positive correction to conductivity which is directly proportional to T, while interelectron interference contributes a negative correction to the conductivity which depends on $T^{-1/2}$. Plotting $1/R$ as a function of $\ln T$ for both films, therefore, would have revealed their dimension. It would be unsurprising if a plot of $1/R_\perp$ versus $\ln T$ was

linear, because the two dimensional behavior of thin films is well established. However, a plot of $1/R_{\|}$ versus $\ln T$ diverging from linear behavior (as discussed previously), would suggest that the widely spaced rows of metallic grains act as a series of one dimensional systems, which would be a novel result. Future investigation could also consider varying the film thickness, because as discussed previously, the formation of the rows of grains is sensitive to the amount of metal evaporated. Grain formation is also sensitive to the surface energy of the film-substrate and film-vapor interfaces, so changing the metal evaporated could also produce different results for the conductivity. If there proves to be a one to two dimensional transition in films evaporated onto angled AAO substrates, these types of systems could provide a vehicle for studying the properties of conductivity in different dimensions.

References

[1] G. Bergmann. Weak anti-localization—an experimental proof for the destructive interference of rotated spin 12. *Solid State Communications*, 42(11):815 – 817, 1982.

[2] V.F. Gantmakher. *Electrons and Disorder in Solids*. Oxford: Oxford University Press, 2005.

[3] Sun-Kyu Hwang, Soo-Hwan Jeong, Hee-Young Hwang, Ok-Joo Lee, and Kun-Hong Lee. Fabrication of highly ordered pore array in anodic aluminum oxide. *Korean Journal of Chemical Engineering*, 19(3):467–473, 2002.

[4] B. Y. Jin and J. B. Ketterson. Dimensional crossover of weak-localization and interaction effects in $nb_{0.53}ti_{0.47}$-ge multilayers. *Phys. Rev. B*, 33:8797–8799, Jun 1986.

[5] Hiroshi Kamimura and Hideo Aoki. *The Physics of Interacting Electrons in Disordered Systems*. Oxford University Press, 1989.

[6] D. S. McLachlan. Weak-localization, spin-orbit, and electron-electron interaction effects in two- and three-dimensional bismuth films. *Phys. Rev. B*, 28:6821–6832, Dec 1983.

[7] Tyuzi Ohyama, Minoru Okamoto, and Eizo Otsuka. Weak localization and correlation effects in indium-tin-oxide films. ii. two-to-three dimensional transition and competition between localization and superconductivity. *Journal of the Physical Society of Japan*, 54(3):1041–1053, 1985.

[8] Niravun Pavenayotin, M. D. Stewart, James M. Valles, Aijun Yin, and J. M. Xu. Spontaneous formation of ordered nanocrystal arrays in films evaporated onto nanopore array substrates. *Applied Physics Letters*, 87(19):193111, 2005.

[9] JA Venables and GDT Spiller. Nucleation and growth of thin films. In *Surface Mobilities on Solid Materials*, pages 341–404. Springer, 1983.

[10] Hylton White and Gerd Bergmann. Localization in near-monolayer films. *Phys. Rev. B*, 40:11594–11602, Dec 1989.

[11] Xue Zhang, James C Joy, Chenwei Zhao, Jin Ho Kim, Gustavo Fernandes, JM Xu, and James M Valles Jr. Evaporating metal nanocrystal arrays. *Nanotechnology*, 28(10):105302, 2017.

A Labview Code

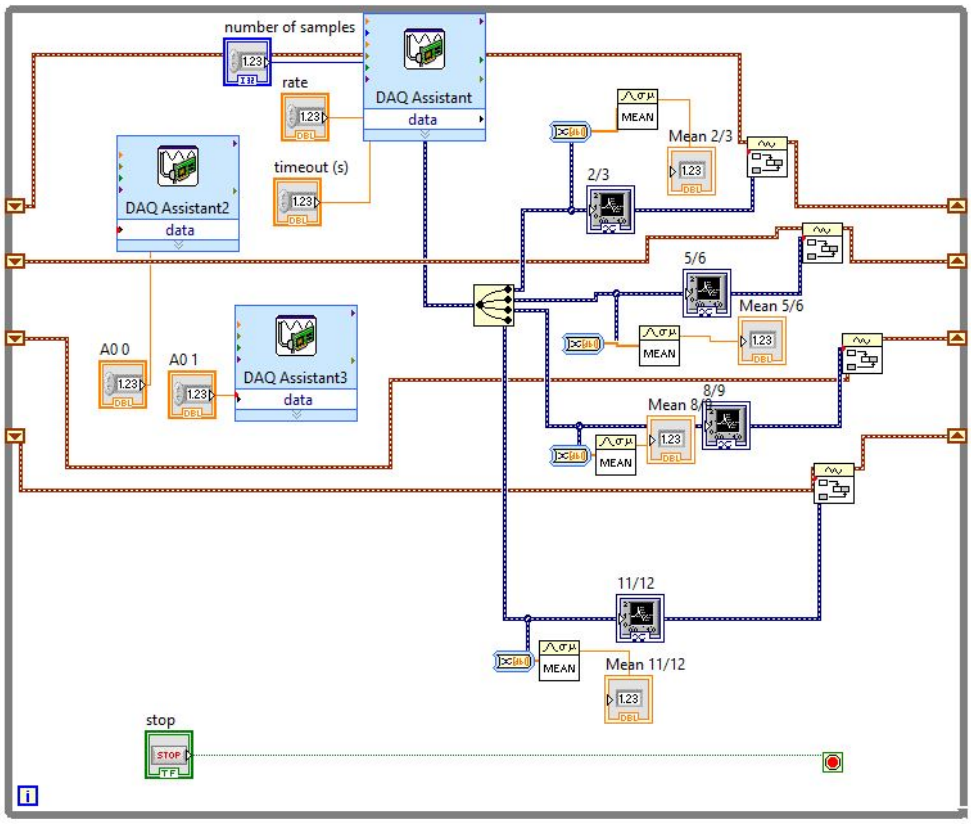

(a)

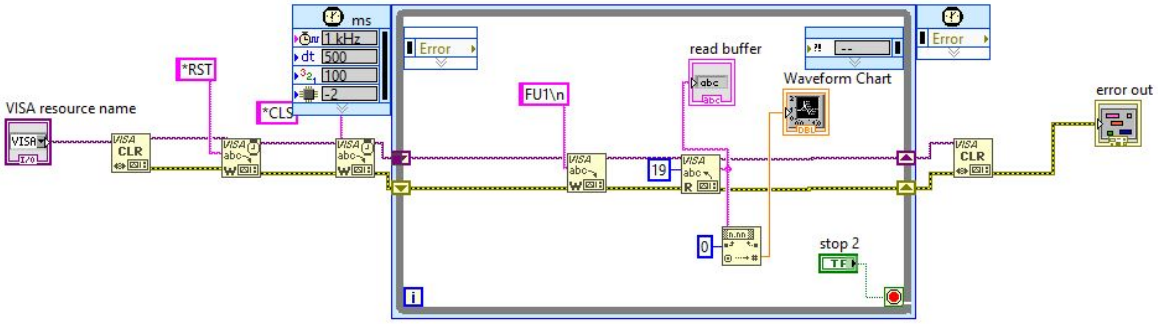

(b)

Figure 13: (a) Labview code for measuring voltage across shunt resistor, thermometer, and two films as a function of time; (b) Labview code for measuring resonant frequency of the quartz crystal as a function of time